Electrochemical mechanisms of Robinia pseudoacacia restoration affecting the interfacial reaction of base cations in loess hilly areas

Catena

Zhou, Zhiying; Yang, Yajun; Yang, Yizhe; Chang, Bokun; Yang, Xiaodong et al

https://doi.org/10.1016/j.catena.2024.108143

Catena 243 (2024) 108143

Contents lists available at ScienceDirect

Catena

journal homepage: www.elsevier.com/locate/catena

Electrochemical mechanisms of *Robinia pseudoacacia* restoration affecting the interfacial reaction of base cations in loess hilly areas

Zhiying Zhou [a,1], Yajun Yang [a,b,1], Yizhe Yang [c], Bokun Chang [a], Xiaodong Yang [a], Gang Cao [a,d], Feinan Hu [e], Chenyang Xu [a,b], Xiaoli Liang [f], Ling Qiu [g], Jialong Lv [a,b], Wei Du [a,b,*]

[a] College of Natural Resources and Environment, Northwest A&F University, Yangling 712100, China
[b] Key Laboratory of Plant Nutrition and the Agro-environment in Northwest China, Ministry of Agriculture, Yangling 712100, China
[c] Cultivated Land Quality and Agricultural Environmental Protection Workstation, Xi'an, Shaanxi Province 710000, China
[d] Soil Physics and Land Management Group, Wageningen University & Research, 6708 PB Wageningen, the Netherlands
[e] College of Soil and Water Conservation Science and Engineering (Institute of Soil and Water Conservation), Northwest A&F University, Yangling, Shaanxi 712100, China
[f] Agricultural Technology Extension Center of Xifeng District, Qingyang, Gansu 745000, China
[g] College of Mechanical and Electronic Engineering & Northwest Research Center of Rural Renewable Energy, Exploitation and Utilization of Ministry of Agriculture, Northwest A&F University, Yangling 712100, China

ARTICLE INFO

Keywords:
Vegetation restoration
Surface electrochemical properties
Specific surface area
Adsorption kinetics
Ion-soil particle surface interaction
Diffusion activation energy

ABSTRACT

Vegetation restoration is an effective strategy for restoring soil function and improving soil quality in ecologically fragile areas; both soil nutrient conservation and interfacial transport are profoundly affected by it. However, reports elucidating the impacts of this on ion adsorption at the soil-water interface from an electrochemical perspective are scarce. This study selected soils from artificial *Robinia pseudoacacia* forests of different ages in the loess hilly region, with cropland serving as the control, to investigate changes in soil basic physicochemical properties, surface electrochemical properties, and the adsorption processes of cations (Na^+, Ca^{2+}, and Mg^{2+}) at the soil-water interface, as well as the intrinsic relationships among these factors. Results show that soil surface charge number (SCN) and specific surface area (SSA) increase with the planting years of vegetation, while the electric field strength (E) decreases. Clay, silt, and organic matter are the major contributing factors to the changes in soil surface electrochemical properties during vegetation restoration, which in turn drive the response of base-cation interface adsorption kinetics. For a given cation type, the adsorption rate constants and equilibrium adsorption amounts increase with increasing SCN and SSA. The electrostatic adsorption energy between ions and soil surfaces increases with the years of vegetation restoration, with the greatest increase in energy proportion for Na^+ (3.037 %), Ca^{2+} (1.805 %), and Mg^{2+} (1.670 %). Correspondingly, the diffusion activation energy involved in ion interface adsorption reaction kinetics decreases with the increase in vegetation restoration years, leading to more thorough ion exchange adsorption reactions and larger equilibrium adsorption amounts. The diffusion activation energy sequence for ions is $Na^+ > Mg^{2+} > Ca^{2+}$, while the observed sequence for cation equilibrium adsorption amounts is $Ca^{2+} > Mg^{2+} > Na^+$. This study provides model predictions and scientific references for nutrient conservation and interfacial transport during the vegetation restoration process.

1. Introduction

Vegetation restoration remains one of the primary strategies for controlling soil erosion and ecosystem rehabilitation in the ecologically fragile areas of the Loess Plateau in China (Liu et al., 2020a; Ma et al., 2022). The widespread implementation of this measure has provided numerous scientific assertions within research fields that affect soil quality and functionality in the Loess Plateau, such as preventing soil erosion (Lei et al., 2012; Zhang et al., 2011), increasing soil carbon sequestration (Deng et al., 2014; Lal, 2002), improving soil nutrient status (Cao et al., 2008; Wang et al., 2011), and enhancing microbial properties (Fu et al., 2009; Zhang et al., 2016), thereby offering

* Corresponding author at: College of Natural Resources and Environment, Northwest A&F University, Yangling 712100, China.
E-mail address: weidu@nwafu.edu.cn (W. Du).
[1] Zhiying Zhou and Yajun Yang contributed equally to this paper.

https://doi.org/10.1016/j.catena.2024.108143
Received 3 February 2024; Received in revised form 13 May 2024; Accepted 28 May 2024
Available online 4 June 2024

extensive practical evidence for supporting the high-quality ecological development of the Yellow River Basin. Ion-surface interactions occurring near the soil–water interface often serve as the controlling intrinsic factors for critical soil processes that affect soil structure and function, such as nutrient retention capacity (Du et al., 2021; Liu et al., 2019), soil water transport (Liu et al., 2020b), aggregate stability (Li et al., 2023c; Li et al., 2022; Liu et al., 2022), and colloid flocculation (Li et al., 2023b). In previous reports, the impact of vegetation restoration on optimizing soil structure and enhancing soil erosion resistance has remained a research focus (Akpa et al., 2014; Ließ et al., 2012). Yet, studies on the response of the ion adsorption micro-processes based on ion-surface interactions at the soil–water interface during vegetation restoration are relatively insufficient. This seems to limit, to a certain extent, the establishment of the intrinsic connection between ion interface reactions at the micro-scale and vegetation restoration at the macro-scale.

Soil nutrient status is the external manifestation of numerous micro-scale processes at the soil–water interface, including ion adsorption, and is significantly influenced by vegetation coverage. The return of nutrients to the soil through the decomposition of plant litter is a key link in the material circulation and energy flow of ecosystems (Li et al., 2015). For instance, the rhizosphere effect plays an essential role in regulating soil organic matter and nutrient cycling (Dijkstra et al., 2013; Han et al., 2020; Wang et al., 2021). The nutrient demand of rhizosphere microorganisms can stimulate their biological activity, release extracellular enzymes to decompose organic matter, promote soil nitrogen availability, and increase soil carbon mineralization and net nitrogen mineralization rates (Ma et al., 2023). Sustained vegetation restoration results in increased soil organic carbon and total nitrogen content, leading to more stable soil nutrients (Huang et al., 2020; Li et al., 2012; Zuo et al., 2009). Precipitation-related changes in soil water content are crucial for preserving soil nutrient cycling and dynamic balance. Precipitation plays an important role in soil nitrogen transformation by directly changing the soil nitrogen cycle through leaching and affecting soil water availability, and indirectly affecting the nitrogen cycle through regulating plant nutrient uptake and productivity (Lv et al., 2021). The change in precipitation pattern indirectly affects the net nitrogen conversion of soil by changing soil properties, vegetation characteristics, and soil nitrate and ammonium nitrogen concentrations (Lv et al., 2023). The increase in soil water-soluble organic carbon and nitrogen reduces microbial metabolic constraints (Zhong et al., 2017) and enhances the availability of soil phosphorus components (Deng et al., 2019; Wang et al., 2023). These studies all indicate that vegetation restoration positively affects both organic and inorganic soil nutrients. Base cations, such as Na^{+}, Mg^{2+}, and Ca^{2+}, are the primary monovalent ions in the soils of Chinese Loess hilly regions. They are not only major sources of soil nutrients but also play crucial roles in affecting soil salinization processes (Jin et al., 2019) and groundwater environmental quality (Su et al., 2021). Many studies show that the total number of base cations increases during vegetation restoration due to the accumulation of litter metabolites in the growth cycle, which also increases the content of exchangeable cations (Sparrius et al., 2012; Vittori Antisari et al., 2013). However, these studies neglect the characterization of ion adsorption behavior. While there are reports on the influence of vegetation restoration on soil ion adsorption capacity, ion migration, and morphological changes of adsorbed ions (Li et al., 2023a; Long et al., 2024; Wen et al., 2023; Yang et al., 2018), in-depth studies on the response mechanisms of ion adsorption characteristics to vegetation restoration measures are still lacking.

It is well known that the surface of soil particles carries a large number of negative charges; hence, the adsorption behavior of positively charged cations at interfaces is inevitably closely related to the surface electronegativity of the soil. Charge characteristics are the foundation of all chemical reactions in the soil and are deeply influenced by its physicochemical properties. Bronick and Lal (2005) have pointed out that soil type and texture shape the characteristics of particle surface charges. Ersahin et al. (2006) evaluated the fractal dimension (Ds) of particle size distribution and its relationship with SSA and SCN. They successfully described the relationship between Ds and SSA or SCN using a second-order polynomial regression equation. Gruba and Mulder (2015) showed that the cation exchange capacity increases with an increase in organic matter content. Many such findings consistently confirm that factors such as vegetation, soil texture, and organic matter can regulate the charge properties of soil surfaces. More in-depth reports indicate that vegetation restoration measures can indirectly control soil charge characteristics by affecting soil texture and organic matter (Liu et al., 2020a; Ma et al., 2022). On one hand, vegetation growth can effectively promote soil clayification, reducing the loss of soil fine particles (Wang et al., 2018); the enriched silt and clay particles can effectively promote an increase in soil surface charge number and specific surface area (Liu et al., 2022). On the other hand, vegetation increases the content of soil organic matter through litterfall and root exudates (An et al., 2009; Bardgett and Wardle, 2003; Jiao et al., 2011; Zhou et al., 2023). The humic substances, which account for over 90 % of soil organic matter, are an important source of variable charges, effectively changing the charge properties of the soil surface (Oorts et al., 2003). Given the significant influence of vegetation restoration on soil physicochemical properties and charge characteristics, it can be speculated that there will be differences in the interfacial adsorption reaction characteristics of base cations at the microscale during this process. Elucidating the impact of vegetation restoration in the Loess hilly regions on the interfacial reaction characteristics of soil base cations will provide a theoretical basis and approach to exploring and resolving environmental issues such as soil nutrient restoration in erosion-prone ecologically fragile areas.

The soil–water interface is the core region for ion adsorption; hence, changes in the interface environment will inevitably cause significant perturbations to ion adsorption behavior, thereby affecting the soil's nutrient retention and supply capacity. Li et al. (2010) found that the abundance of negative charges on the soil surface can create a strong electric field of 10^{8} V m^{-1} near the soil surface. Under the influence of this electric field, ion exchange adsorption occurring at the soil–water interface is essentially an ion diffusion process driven by an electric potential gradient and activity gradient, based on which an ion adsorption diffusion model in a non-ideal system under an external electric field was established (Li et al., 2011b). Du et al. (2016) have discovered that under the influence of surface electric fields, the adsorption kinetics of alkali metal ions on clay mineral surfaces will show significant differences. In a strong electric field, ions show zero-order kinetics during adsorption diffusion to charged surfaces, influenced by strong electrostatic forces. Here, the ion adsorption rate remains constant, regardless of the amount adsorbed. Conversely, in a weak electric field, ion adsorption diffusion near the interface exhibits first-order kinetics, governed by weaker electrostatic forces, and the adsorption rate decreases as more ions are adsorbed. This mechanistic model utilizes several parameters, including ion adsorption kinetic reaction order, adsorption rate, and equilibrium adsorption amount, to comprehensively reflect the electrochemical relationship between soil surface charge characteristics and ion interface reaction properties (Deng and Li, 2022; Du et al., 2017; Du et al., 2019; Du et al., 2020; Li et al., 2021b). However, studies exploring the response of base cation adsorption kinetics at the soil–water interface to vegetation restoration measures based on soil electric field theory have not yet been disclosed, undoubtedly creating obstacles for establishing the link between the macroscopic ecological restoration process in the Loess hilly regions and the microscopic interfacial processes of soil nutrients.

Accordingly, this study selects soil from artificial *Robinia pseudoacacia* plantation areas with different ages in the Loess hilly region, and cropland soil as the control, to conduct research on varying soil physicochemical properties, surface electrochemical attributes, and the adsorption kinetics of base cations Na^{+}, Ca^{2+}, and Mg^{2+}. The objective is to elucidate: (1) the physicochemical properties and surface

electrochemical attributes of *Robinia pseudoacacia* soils of different ages, as well as the interrelation between them; (2) the characteristics of base cation adsorption kinetics on the surface of *Robinia pseudoacacia* soils with different ages; and (3) the electrochemical driving mechanisms for the base cation adsorption characteristics at the soil–water interface. The research findings aim to provide model predictions and scientific assessments for the dependability of nutrient interfacial transport in the soil of the Loess Plateau during the process of vegetation restoration.

2. Materials and methods

2.1. Study area overview

The test soil samples for this study were collected from artificial *Robinia pseudoacacia* forests in Ansai District, Yan'an City, Shaanxi Province (109°19′23″ E, 36°51′30″ N). *Robinia pseudoacacia*, a nitrogen-fixing tree, is a promising afforestation for controlling soil and water erosion. Introduced in the 1950 s, it covers more than 70,000 acres on the Loess Plateau. Studies show it influences soil moisture, structure, chemical characteristics, respiration, and enzyme activity (Zhu et al., 2019). However, few studies have focused on its impact on nutrient ion interfacial transport. Ansai is located in the hinterland of the Loess Plateau, belonging to the typical loess hilly and gully region, in the transition climate from warm temperate semi-humid to semi-arid. The region experiences dry and windy conditions in spring, hot and rainy summers, and dry and cold winters, with an average annual temperature of 8.8 °C and an average annual rainfall of 540 mm. The area is a transitional zone between loessial soil and sandy loess, with zonal soil being dark loessial, most of which has eroded away, showing widespread exposure of the loess parent material, primarily loessial soil. The vegetation zoning belongs to the transition from warm temperate deciduous broadleaf forest to dry steppe and forest steppe areas, with the original vegetation no longer existing. The current natural secondary vegetation is mainly composed of herbaceous communities dominated by species such as *Bothriochloa ischaemum*, *Stipa bungeana*, *Artemisia gmelinii*, and *Artemisia giraldii*, along with sporadic mixed shrubbery; artificial forest and grasslands primarily include *Robinia pseudoacacia*, *Caragana korshinskii*, *Hippophae rhamnoides*, *Astragalus huangheensis*, *Alfalfa*, and *Lespedeza*.

2.2. Sample collection and preparation

After field reconnaissance, artificial *Robinia pseudoacacia* forests of 21 and 53 years of age were selected, with neighboring cropland serving as the control. Soil collection points with similar site conditions (i.e., slope and aspect) were chosen, performing 3 replicated random samplings at each site. The surface layer of soil (0–20 cm) was collected after clearing dead branches and leaves, air-dried, and stored at room temperature. Each soil sample was divided into three parts, which were sieved through a 2 mm screen to remove plant roots for analysis of basic properties, surface electrochemical properties, and adsorption kinetics experiments.

2.3. Determination of soil basic physicochemical properties and surface electrochemical properties

The physical and chemical properties of the soil were determined using standard methods. The pH of the soil suspension at a 1:2.5 soil-to-water ratio was measured with a pH electrode (Sumner and Miller, 1996). The soil calcium carbonate content was determined using the gasometric method. Soil organic matter (SOM) was determined by potassium dichromate oxidation (Nelson and Sommers, 1983). After the removal of soil organic matter with hydrogen peroxide and calcium carbonate with hydrochloric acid (Yang et al., 2015), the soil mechanical composition was determined by the pipetting method and classified according to the USDA soil taxonomy. Soil samples, pre-treated through a 200-mesh, were analyzed for soil mineral types and content using X-ray diffraction (XRD) (Rigaku/D Max-A, Japan) (Tsao et al., 2013).

The specific surface area and surface electrochemical properties of the soil were determined using the combined determination method proposed by (Li et al., 2011a). Approximately 100 g of soil was washed four times with 0.5 mol/L HCl to prepare H^+-saturated samples, followed by repeated rinsing with deionized water until the suspension was free of Cl^- (indicated by no white precipitate forming when a small amount of suspension was combined with a 50 g/L $AgNO_3$ solution). The H^+ saturated samples were dried and sieved through a 0.25-mm screen. Then, 10 g of H^+ saturated soil sample was transferred to a conical flask, and a mixed solution of 0.0075 mol/L $Ca(OH)_2$ and NaOH was added. After shaking for 24 h, the pH of the suspension was adjusted to 7 with 1 mol/L HCl. The suspension was then shaken for another 24 h to reach ion exchange equilibrium, and the final pH value, approximately 7, was determined. After centrifugation, the supernatant was collected and the concentrations of Ca^{2+} and Na^+ were measured with a flame photometer. Each experimental group included three replicates, each of which was measured three times to calculate the average value. Using the obtained experimental data in conjunction with the combined determination method, electrochemical parameters of the test soil, such as specific surface area, surface charge number, surface potential (φ), surface electric field, and surface charge density (σ), were obtained.

2.4. Ion adsorption kinetics experiments

In this study, the miscible displacement technique (Li et al., 2011c; Liu et al., 2023) was employed to carry out ion adsorption kinetics experiments. Soil samples were pre-saturated with K^+ using a 0.1 mol/L KCl solution and then dried at 60 °C before being sieved through a 0.25 mm mesh. A total of 0.5 g of K^+ saturated sample was evenly spread in the exchange column. To eliminate the effects of ion diffusion caused by the longitudinal concentration gradient, the thickness of the sample should be as thin as possible (in this study, 0.02–0.03 cm). The spread area of the samples was approximately 15 cm^2. Exchange solutions of NaCl, $CaCl_2$, and $MgCl_2$ at predetermined concentrations (0.1, 1, 10 mmol/L) were passed through the soil samples at a constant flow rate of 0.5 ml min^{-1} at room temperature (298 K), with an automatic collector (DBS100, QPHX Instrument Co., Ltd., Shanghai, China) collecting the effluent every 5 min into tubes. The concentrations of Na^+, Ca^{2+}, and Mg^{2+} in the exchange and effluent solutions were determined using a flame photometer (PinAAcle 900F, PerkinElmer Inc., USA). The amounts of Na^+, Ca^{2+}, and Mg^{2+} adsorbed on the soil surface were calculated based on the concentration difference before and after adsorption.

The investigations by Li et al. (2010) and Li et al. (2011c) have revealed that if a strong electric field exists on the surface of soil particles, the ion adsorption kinetics exhibit the characteristics of zero-order kinetics dominated by strong adsorption effects:

$$\frac{dN_i(t)}{dt} = k_{i(0)} N_i(t)^0 \tag{1}$$

where $N_i(t)$ is the amount of ith ion adsorbed at time t during the adsorption/diffusion process; $k_{i(0)}$ is the zero-order adsorption rate constant, and:

$$k_{i(0)} = \frac{\pi^2 D_{i0}}{2l^2} SSA f_{i0} \exp^{-\frac{Z_i F \varphi}{2RT}} \tag{2}$$

where π is the circular ratio; D_{i0} is the diffusion coefficient of ith ion; l is the diffusion distance of ion in the double layer; SSA is the specific surface area of the sample; f_{i0} is the initial concentration of ith ion; Z_i is the ionic charge number; F is the Faraday constant; φ is the surface potential; R and T are the gas constant and absolute temperature, respectively.

When the strong adsorption force between the ions and the surface

acts to saturation, the ions will continue to diffuse under the influence of a weaker adsorption force. The diffusion distance will be reduced from 0-*l* to 0-*l*'. At this point, the kinetic adsorption process exhibits first-order kinetic characteristics:

$$\frac{dN_i(t)}{dt} = k_{i(1)}\left[1 - \frac{N_i(t)}{N_i(t\to\infty)}\right] \tag{3}$$

where $N_i(t\to\infty)$ represents the equilibrium adsorption quantity of *i*th ion; $k_{i(1)}$ is the first-order adsorption rate constant, and it is given by:

$$k_{i(1)} = \frac{\pi^2 D_{i0}}{2l^2} SSAf_{i0}\exp^{-\frac{Z_i F\varphi}{2RT}} \tag{4}$$

The equilibrium adsorption quantity $N_i(t\to\infty)$ is:

$$N_i(t\to\infty) = 2SSAlf_{i0}\exp^{-\frac{Z_i F\varphi}{2RT}} \tag{5}$$

According to equations (1) and (3), the cation adsorption kinetics curves of $N_i(t)/dt$ and $N_i(t)$ as shown in Fig. 1 can be drawn, where $N_i(t)$ represents the adsorption capacity and $N_i(t)/dt$ represents the adsorption rate. If there is a strong adsorption force in the ion-surface interactions, the relationship between adsorption rate and adsorption amount will show two straight lines, as shown in Fig. 1A. If only a weak adsorption force exists in the ion-surface interactions, the plot of adsorption rate and adsorption amount will present a single straight line, as shown in Fig. 1B (Du et al., 2017). When the adsorption reaches complete equilibrium, the ion adsorption rate is zero, and the adsorption amount reaches its maximum.

For convenience in utilizing experimental data, Eqs (1) and (3) are respectively represented in differential form as follows:

$$\frac{N_i(t_{m+1}) - N_i(t_m)}{t_{m+1} - t_m} = k_{i(0)} \tag{6}$$

$$\frac{N_i(t_{m+1}) - N_i(t_m)}{t_{m+1} - t_m} = k_{i(1)}\left[1 - \frac{N_i\left(t_{m+\frac{1}{2}}\right)}{N_{i(t\to\infty)}}\right] \tag{7}$$

where $m = 1, 2, 3\ldots$; $N_i(t_{m+1/2}) = N_i(t_m) + 0.5[N_i(t_{m+1})\text{-}N_i(t_m)]$.

For a 1:1-type electrolyte, where the adsorption energy $w_T(0)$ of a monovalent cation on the surface can be expressed as (Li et al., 2021a):

$$w_T(0) = -2RT\ln\frac{N_i(t\to\infty)}{2(SSA/\kappa)a_0} \tag{8}$$

where a_0 is the activity of the cation in the bulk solution, and the Debye parameter κ is defined as:

$$\kappa = \sqrt{\frac{8\pi F^2 a_0}{\varepsilon RT}} \tag{9}$$

where ε is the dielectric constant.

For a 2:1-type electrolyte, where the adsorption energy of a divalent cation on the surface is represented as (Li et al., 2021b):

$$w_T(0) = -2RT\ln\frac{N_i(t\to\infty)}{\sqrt{3}(SSA/\kappa)a_0} \tag{10}$$

where the Debye parameter κ is:

$$\kappa = \sqrt{\frac{24\pi F^2 a_0}{\varepsilon RT}} \tag{11}$$

In accordance with the double electric layer theory, the exchange ions must surmount the energy potential barrier generated by the interactions between the ions in the adsorbed state and the surface of soil particles to achieve complete adsorption or diffusion onto the surface of soil colloidal particles. The energy necessary to overcome this barrier is referred to as the diffusion activation energy for the exchange ions (ΔE_i). In light of the ion adsorption rate equation and the expression for the equilibrium adsorption quantity, along with the incorporation of the Arrhenius equation (Jardine and Sparks, 1984), it follows:

$$\Delta E_i = RT[\ln SCN - \ln N_i(t\to\infty)] \tag{12}$$

2.5. Data analysis

The basic physicochemical properties and surface electrochemical properties of soils in different-aged *Robinia pseudoacacia* plantation areas were analyzed using variance analysis with SPSS 26 software. The relationship between the basic physicochemical properties and the surface electrochemical properties of soil was examined through Pearson correlation tests. Redundancy analysis (RDA) between soil surface electrochemical properties and the adsorption kinetic parameters of exchangeable cations on soil particle surfaces was conducted using Canoco5 software.

3. Results

3.1. Characteristics of soil physicochemical property evolution in Robinia pseudoacacia plantations of different ages

By examining the basic physicochemical properties of the soil at a depth of 0–20 cm from both the control cropland and *Robinia*

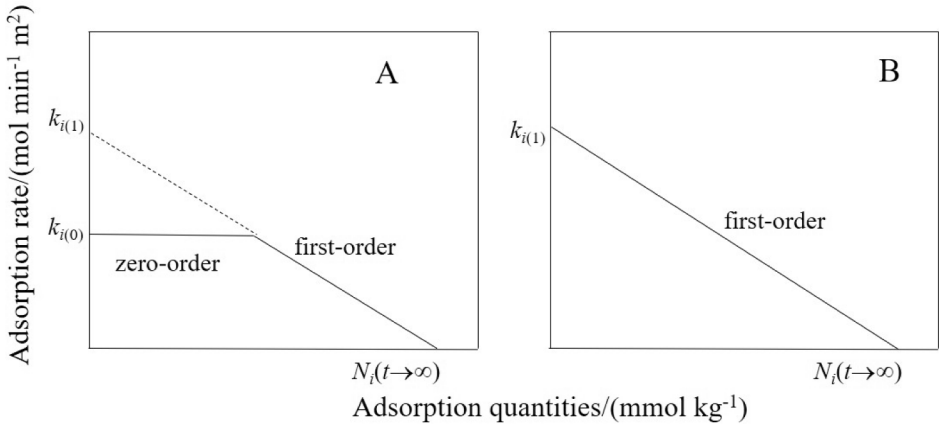

Fig. 1. Schematic diagram of ionic adsorption kinetic curves governed by strong adsorption force (A: zero-order and first-order) and weak adsorption force (B: first-order), respectively.

pseudoacacia plantations of varying ages (as shown in Table 1), it is evident that with the prolonged cultivation of *Robinia pseudoacacia*, there is a general decreasing trend in the soil pH and $CaCO_3$ content. The soil organic matter (SOM) content demonstrates a significant increase as the restoration period lengthens ($P < 0.05$), with the 21-year and 53-year *Robinia pseudoacacia* plantation soils having SOM contents 1.28 and 2.17 times greater than those of the control cropland soils, respectively. When compared to the cropland, the soil sand content in the 21-year and 53-year *Robinia pseudoacacia* plantation areas was reduced by 9.16 % and 11.45 %, respectively, while silt content increased by 11.36 % and 18.30 %, respectively, and clay content decreased by 19.37 % and 37.45 %, respectively. Although there were certain changes in the soil particle content during the restoration process, the soil texture in this area predominantly remained as loam. Specifically, soil from the 53-year-old *Robinia pseudoacacia* plantation area exhibited the highest silt content and the lowest clay content of 62.39 % and 10.17 %, respectively.

The soil mineral composition and content, as indicated in Table 2, remained relatively consistent with an increase in the age of the *Robinia pseudoacacia* plantations. The primary minerals are mainly quartz and feldspar. Furthermore, the presence of a wide array of rich clay minerals is also noted, principally consisting of illite, chlorite, montmorillonite, vermiculite, and kaolinite, all representing over 60 % of the total mineral content.

3.2. Evolutionary characteristics of soil surface electrochemical properties in different-age Robinia pseudoacacia plantation areas

The soil surface electrochemical parameters of different-age *Robinia pseudoacacia* plantation areas are listed in Table 3. As shown in Table 3, SSA follows the sequence of cropland < 21-year soil < 53-year soil, with the SSA of the 21-year and 53-year soils increasing by 44.67 % and 50.99 %, respectively, compared to cropland ($P < 0.05$). The trend of SCN in the topsoil of cropland and artificial *Robinia pseudoacacia* forest follows the same sequence as SSA, which is cropland < 21-year soil < 53-year soil; however, the difference between 21 and 53 years is not significant. The highest E is observed in croplands and decreases with the age of the artificial forest, showing the sequence of cropland > 21-year soil > 53-year soil. The φ varies between 80.68–84.64 mV, with an average value of 82.35 mV. The σ ranges from 0.14-0.18C/m^{-2}(−|-), with the maximum value recorded in cropland.

3.3. Correlation between basic physicochemical properties and electrochemical properties

The correlation between the basic physicochemical properties (listed in Table 1) and the electrochemical properties (listed in Table 3) of soil was analyzed, with the results shown in Fig. 2. Fig. 2 reveals that SCN is positively correlated with SOM and silt content, with a significant correlation ($P < 0.05$). SSA is significantly positively correlated with silt content ($P < 0.01$) and shows a positive correlation with SOM, though less strong, while it is highly negatively correlated with clay content ($P < 0.01$). E is positively correlated with SOM, but the correlation is weak, and it is highly significantly positively correlated with silt content ($P < 0.01$), whereas it has a significant negative correlation with clay content ($P < 0.01$). Both φ and σ are negatively correlated with silt content ($P < 0.05$) and positively correlated with clay content ($P < 0.05$).

Table 1
Basic physical and chemical properties of different soil samples.

Sample	pH	$CaCO_3$ (g kg^{-1})	SOM (g kg^{-1})	Particle size distribution		
				Sand(%)	Silt(%)	Clay(%)
Cropland	8.34 ± 0.02c	90.1 ± 0.13b	5.05 ± 0.54c	31 ± 0.48a	52.74 ± 0.18a	16.26 ± 0.31a
21-Yr soil	8.48 ± 0.01a	96.65 ± 0.95a	6.47 ± 0.41b	28.16 ± 7.32a	58.73 ± 8.6a	13.11 ± 1.28b
53-Yr soil	8.41 ± 0.01b	82.83 ± 2.22c	10.97 ± 0.12a	27.45 ± 0.87a	62.39 ± 0.96a	10.17 ± 0.08c

The results of the redundancy analysis (RDA) are depicted in Fig. 3. Axis 1 (67.29 %) and Axis 2 (10.33 %) together explained 77.62 % of the total variance, indicating that variations in the basic physicochemical properties of soil lead to changes in its surface electrochemical properties. Clay and silt contents explained 51.2 % and 13.7 % of the variation in surface properties, respectively, as seen in Table 4, suggesting that they are the primary factors influencing the soil's surface electrochemical characteristics. SCN and SSA showed a positive correlation with both SOM content and silt content and a negative correlation with clay content. E, φ, and σ were positively correlated with clay content, sand content, and $CaCO_3$, while showing a negative correlation with silt content.

3.4. Adsorption kinetics of base cations on soil surfaces in Robinia pseudoacacia plantations of different ages

Using equations (6) and (7), the results for the adsorption kinetics of each base cation were obtained, as shown in Fig. 4. Several observations can be made from Fig. 4: (1) In all treatments, the adsorption processes of Na^+, Ca^{2+}, and Mg^{2+} on the soil surface of cropland and *Robinia pseudoacacia* plantations aged 21 and 53 years only exhibited a first-order kinetic process; (2) For the given type of base cation and under specific electrolyte concentration conditions, both the adsorption rate and equilibrium adsorption capacity increased with the age of the *Robinia pseudoacacia* plantation. For example, at 0.1 mmol/L, the adsorption rates and equilibrium adsorption capacities for Na^+ on the soil surface of cropland, 21-year-old and 53-year-old *Robinia pseudoacacia* plantations were 4.715 mmol min^{-1} m^{-2}, 6.674 mmol min^{-1} m^{-2}, 9.561 mmol min^{-1} m^{-2}, and 3.022 mmol kg^{-1}, 3.872 mmol kg^{-1}, and 4.285 mmol kg^{-1}, respectively, following the order of 53-year soil > 21-year soil > cropland; (3) On a given electrolyte concentration and soil type surface, the equilibrium adsorption amounts of the three base cations followed the order of Ca^{2+} > Mg^{2+} > Na^+. The equilibrium adsorption amounts of the ions increased with the increase in electrolyte concentration, but the change in electrolyte concentration did not alter the order of the ion's equilibrium adsorption amounts. For instance, at electrolyte concentrations of 0.1, 1, and 10 mmol/L respectively, the equilibrium adsorption amounts of Ca^{2+}, Mg^{2+}, and Na^+ on soil particle surfaces in a 21-year-old *Robinia pseudoacacia* plantation increased from 3.872, 2.66, and 2.216 mmol kg^{-1} to 30.025, 21.004, and 18.320 mmol kg^{-1}, finally reaching 157.979, 135.663, and 95.753 mmol kg^{-1}.

3.5. Correlation between soil electrochemical properties and ion adsorption kinetic characteristics

Although the ion adsorption kinetic model used in this study is based on soil electric field theory, the correlation analysis between model parameters and soil electrochemical properties is still of general significance. For this purpose, a redundancy analysis was conducted to assess the relationship between soil surface electrochemical properties and ion adsorption kinetic parameters under all treatments, the results of which are shown in Fig. 5. At any given electrolyte concentration, the electrochemical properties explained more than 99 % of the variation in adsorption kinetic characteristic parameters on soil particle surfaces. The equilibrium adsorption amounts and adsorption rate constants of Na^+, Ca^{2+}, and Mg^{2+} were positively correlated with SSA and SCN while negatively correlated with E, φ, and σ, although the contributions of each factor to the adsorption kinetics differed under various electrolyte concentration conditions (Table 5). At an electrolyte concentration of 0.1 mmol/L, SCN was the main contributing factor to the variation in ion adsorption kinetic characteristic parameters, contributing up to 93.6 %, while SSA and φ each contributed 2.6 %; at an increased concentration of 1 mmol/L, SSA and SCN were the major factors affecting the variation

Table 2
Mineral composition of different soil samples.

Sample	Kaolinite	Illite	Chlorite	Montmorillonite	Vermiculite	Feldspar	Quartz
Cropland	+	++++	++	+	+	++	++++
21-Yr soil	+	++++	++	+	+	++	++++
53-Yr soil	+	++++	+++	+	+	++	+++

Note: The symbol "-" indicates not detected; "+" indicates less than 10%; "++" indicates 10%–20%; "+++" indicates 20%–30%; "++++" indicates 30%–40%.

Table 3
Surface electrochemical properties of different soil samples.

Sample	SSA (m^2/g)	SCN (cmol kg^{-1})	E (10^8V/m)	Φ (mV)	σ (C/ m^{-2}(−|-))
Cropland	33.89 ± 1.63e	6.78 ± 1.02c	2.5 ± 0.17a	84.64 ± 1.56a	0.18 ± 0.01a
21-Yr soil	49.03 ± 0.66b	10.54 ± 0.19b	2.01 ± 0.1c	80.68 ± 0.5b	0.14 ± 0.01c
53-Yr soil	51.17 ± 0.65a	14.23 ± 0.23a	1.93 ± 0.03c	81.74 ± 0.28b	0.14c

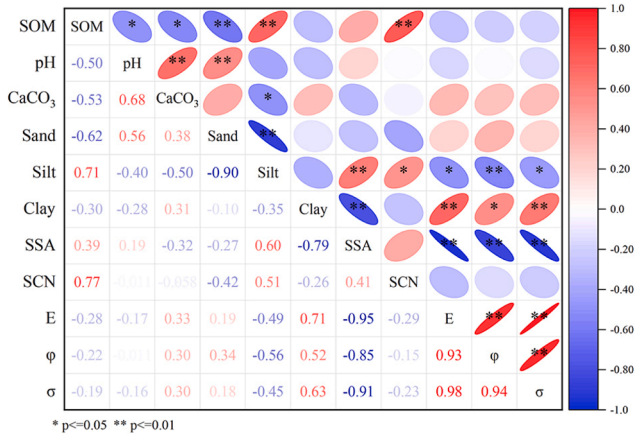

Fig. 2. Correlation of soil surface electrochemical properties with basic physical and chemical properties.

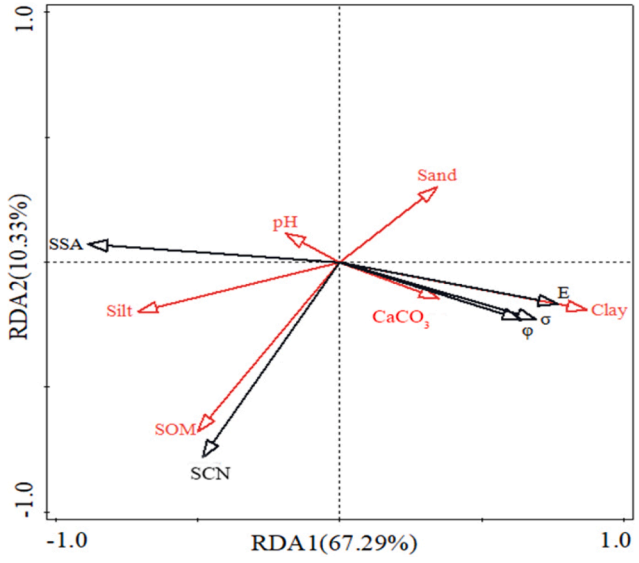

Fig. 3. RDA relationship analysis between basic physicochemical properties of soil and surface electrochemical properties.

Table 4
Factor interpretation rates under redundancy analysis of soil surface electrochemical and physicochemical properties.

Factor	Explains %	F	P
Clay	51.2	19.9	0.002
Silt	13.7	7	0.006
SOM	6.7	4	0.014

in ion adsorption kinetic parameters, contributing 89.9 % and 8.2 %, respectively; when the electrolyte concentration reached 10 mmol/L, SSA explained 95.4 % of the variation in ion adsorption kinetic parameters, while SCN and φ only contributed 3.8 % and 0.5 %.

3.6. *Interaction energy and diffusion activation energy between base cations and soil particles in Robinia pseudoacacia plantations of different ages*

Fundamentally, the differences in the adsorption kinetic characteristics of Ca^{2+}, Mg^{2+}, and Na^{+} ions on the soil surfaces of *Robinia pseudoacacia* plantations of various ages originate from the varied interactions between the exchangeable cations and the surfaces of soil particles. Therefore, based on equations (8) and (10), the interaction energy between the exchangeable cations and soil particle surfaces in *Robinia pseudoacacia* plantations of different ages was calculated, as illustrated in Fig. 6. Fig. 6 reveals three important observations: (1) The interaction energy between the exchangeable cations and soil particle surfaces shows an attractive force; (2) under the same electrolyte concentration conditions, the interaction energies between divalent Ca^{2+} and Mg^{2+} and soil particles are both greater than that of monovalent Na^{+} with soil particles; (3) with a given ion type and electrolyte concentration, the interaction energy between all ions and soil particles increases with the duration of vegetation restoration.

Driven by ion-surface interactions, the salt-base cations in soil solution progressively diffuse towards soil particle surfaces. During the process of the diffusion of base ions from the liquid to the solid phase, an energy barrier generated by exchanged ion-surface interactions (diffusion activation energy) must be overcome (Du et al., 2020). The diffusion activation energy of Na^{+}, Ca^{2+}, and Mg^{2+} on the soil surface can be further calculated according to equation (12), as shown in Table 6. The following three observations can be drawn from Table 6: (1) At the given electrolyte concentration, the diffusion activation energy required for ion adsorption decreases as the forest age of the *Robinia pseudoacacia* increases. For example, at a concentration of 0.1 mmol/L, the required diffusion activation energy for Na^{+} adsorption onto the soil surface follows the following order: cropland soil > 21-year-old *Robinia pseudoacacia* plantations soil > 53-year-old *Robinia pseudoacacia* plantations soil; (2) within the same forest age soil, the required activation energy for ions decreases with increasing electrolyte concentration; (3) at given forest age soil and electrolyte concentration, the activation energy required for Na^{+} is the highest, followed by Mg^{2+} and Ca^{2+}, respectively. For instance, at a concentration of 1 mmol/L, the activation energies required for the adsorption of Na^{+}, Ca^{2+}, and Mg^{2+} on the soil surface of a 53-year-old *Robinia pseudoacacia* plantation are 2.940 kJ mol^{-1}, 2.934 kJ mol^{-1}, and 1.447 kJ mol^{-1}, respectively. However, when the electrolyte concentration increases to 10 mmol/L, as the ion

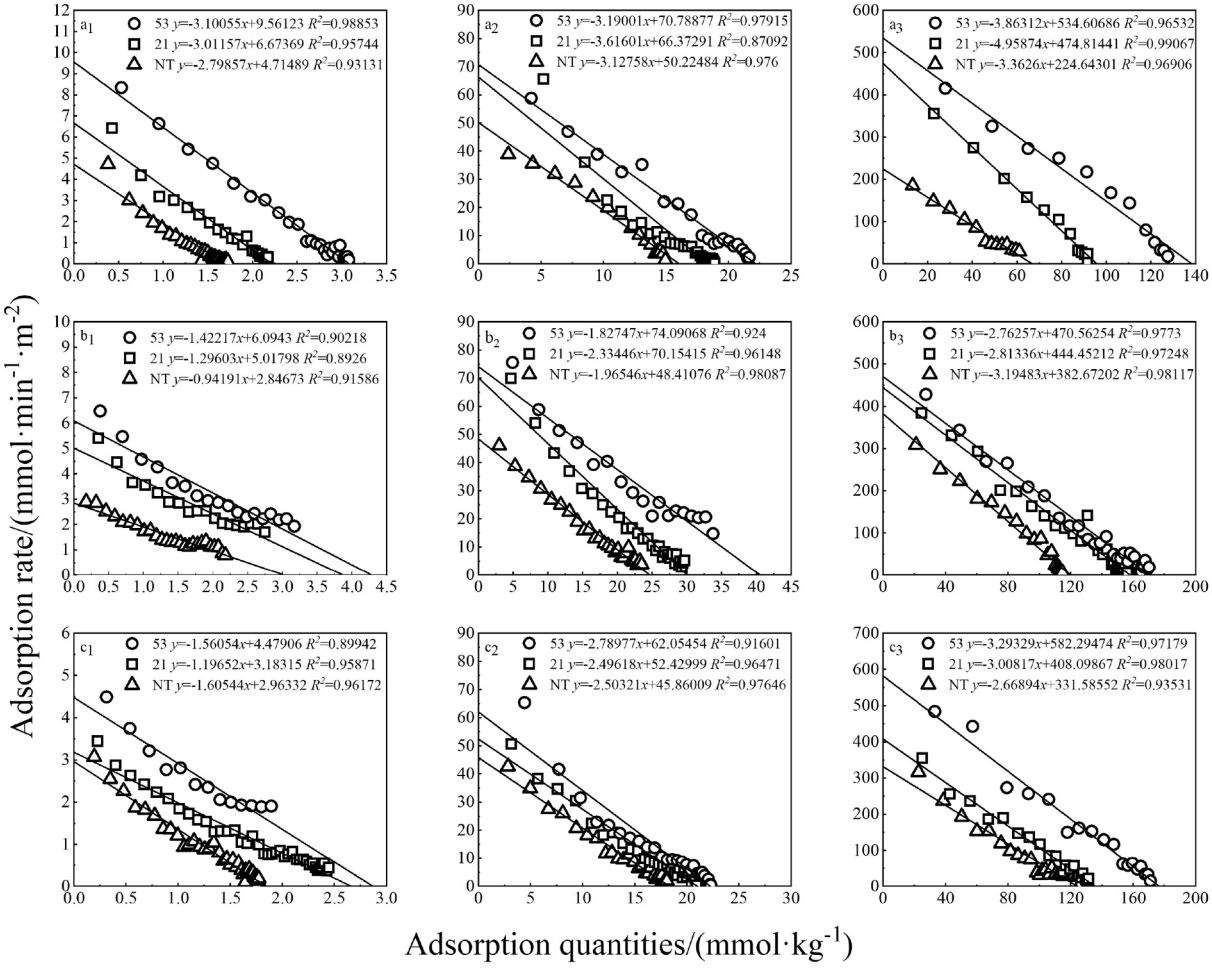

Fig. 4. Adsorption kinetic curves of Na^+ (a), Ca^{2+} (b), and Mg^{2+} (c) at the soil surface of cropland(△), 21-year-old *Robinia pseudoacacia* plantation area(□), and 53-year-old *Robinia pseudoacacia* plantation area(○) under different electrolyte concentrations (1: 0.1 mmol/L, 2: 1 mmol/L, 3: 10 mmol/L).

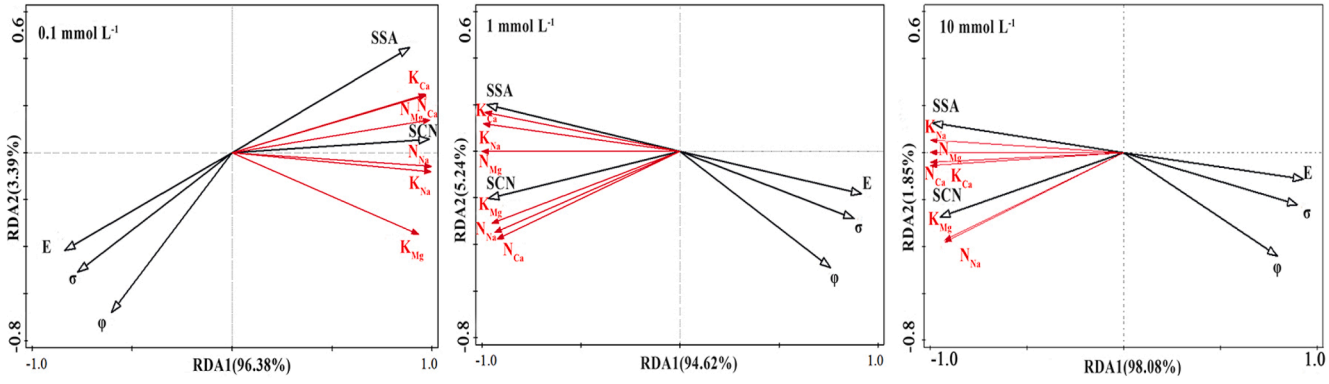

Fig. 5. Redundancy analysis of the relationship between soil surface electrochemical properties and the adsorption kinetic parameters of Na^+, Ca^{2+}, and Mg^{2+}.

exchange adsorption reactions reach a true equilibrium, the diffusion activation energy required for the salt-base cations on the soil surface becomes zero (Du et al., 2020).

4. Discussion

4.1. Impact of artificial Robinia pseudoacacia restoration on the basic physicochemical properties of soil

In this study, significant differences were observed in the basic physicochemical indicators of soils from *Robinia pseudoacacia* plantations of different ages (Table 1), indicating that the duration of restoration plays an important role in the physicochemical properties of soil. Many studies have shown that the process of vegetation restoration increases SOM content (Murty et al., 2002; Tuo et al., 2018; Zhao et al., 2015), which can be attributed to the decomposition and transformation of large amounts of plant litter (An et al., 2009; Van Veen and Kuikman, 1990; Zeng et al., 2018). Compared with cropland, the SOM content in artificial *Robinia pseudoacacia* forests has increased, and it is positively correlated with the age of plantation; the SOM content was 2.17 times

Table 5
Factor interpretation rates under redundancy analysis of soil surface electrochemical characteristics and ion adsorption kinetic parameters.

Factor	f_0(mmol/L)	Explains %	F	P
SSA	0.1	2.6	4.1	0.048
	1	89.9	62.6	0.004
	10	95.4	145	0.004
SCN	0.1	93.6	103	0.004
	1	8.2	26.5	0.004
	10	3.8	27.9	0.002
φ	0.1	2.6	27.3	0.01
	1	1.1	10.4	0.036
	10	0.5	7.4	0.024

higher in a 53-year-old *Robinia pseudoacacia* plantation than in cropland, suggesting that artificial *Robinia pseudoacacia* forests can enhance SOM content. Litterfall, roots, and root exudates have been identified as major sources of SOM during vegetation restoration (An et al., 2009; Chen et al., 2018; Johansson, 1995). It is therefore reasonable to speculate that as the restoration period increases, the organic matter content from the decomposition and transformation of litterfall and other plant residues at the soil surface in *Robinia pseudoacacia* forests gradually increases. With the increasing age of *Robinia pseudoacacia* forests, soil sand content decreases while silt content increases, suggesting that the particle composition of the soil evolves towards finer particles during the vegetation restoration process (Zhai et al., 2020). Increased vegetation cover can slow down erosion by rainfall and surface runoff, protecting soil fine particles from being lost (Gu et al., 2019; Li and Shao, 2006; Wang et al., 2008), while the accumulation of litter during plant growth increases soil fine particle content (Sun et al., 2016). SOM content is negatively correlated with sand content and positively correlated with silt content ($P < 0.01$) (Fig. 2), which could be due to organic matter being predominantly stored within microaggregates, reducing the potential for enzyme and microbial contact with the organic matter, thereby decreasing the turnover rate of organic matter and stabilizing it (An et al., 2010; Shang et al., 2014). Soil pH and the calcium carbonate content decrease as vegetation age increases, displaying a very significant positive correlation ($P < 0.01$), while both are significantly negatively correlated with organic matter ($P < 0.05$) (Fig. 2). Organic matter accumulation plays a crucial role in reducing soil pH and calcium carbonate content, which may be due to the positive effect of nitrification of vegetation litter in reducing soil pH values (Jin et al., 2022), together with the secretion of organic acids by plant roots, which dissolve calcium carbonate and concurrently decrease soil pH (Ghani et al., 2023).

4.2. The intrinsic link between soil physicochemical properties and surface electrochemical properties during artificial Robinia pseudoacacia restoration

4.2.1. Relationship between SOM, SCN, and SSA

Previous studies have shown that SCN increases significantly with the rise in SOM content (Asadu et al., 1997; Kweon et al., 2013; Zhao et al., 2019). Organic matter contributes 75 %-85 % of the soil surface charge (Oorts et al., 2003); even in grassland restoration areas, organic matter contributes 37.5 % of the soil surface charge (Liu et al., 2020a). In this study, we found an extremely significant positive correlation between SCN and SOM with the extension of *Robinia pseudoacacia* forest restoration time ($P < 0.01$) (Fig. 2). This correlation could be due to the presence of polar functional groups on organic matter surfaces; the dissociation and protonation of these groups can generate variable charges and provide substitution sites for cations (Bolan et al., 1999; Saidian et al., 2016). Therefore, the increase in SOM content is an important factor in the augmentation of SCN during the *Robinia pseudoacacia* forest restoration process. The SSA also increases with SOM content during the restoration process of *Robinia pseudoacacia* forests. This might be attributed to SOM possessing high specific surface area (Pennell et al., 1995); the intrinsic nature of high surface area dictates the positive relationship between them (Liu et al., 2020a; Ma et al., 2022; Yu et al., 2017).

4.2.2. Relationship between silt and clay content and SCN and SSA

Correlation analyses (Fig. 2) and redundancy analysis (Fig. 3) suggest that during the artificial *Robinia pseudoacacia* restoration process, SCN and SSA have a positive correlation with silt content (contributing 13.7 %) and a negative correlation with clay content (contributing 51.2 %). The influence of silt on SCN might stem from its richness in phyllosilicate minerals that carry a greater charge (Iturri and Buschiazzo, 2014). As shown in Table 2, the soil was composed of 30 %-40 % illite, a mineral typically found in medium and fine silt fractions, conducive to charge generation (Soares et al., 2005). SSA is dependent on the quantity

Table 6
Activation energies of Na^+, Ca^{2+}, and Mg^{2+} at the soil surface.

Sample	f_0((mmol/L) (mmol/L)	ΔE_{Na}(kJ/mol) (kJ/mol)	ΔE_{Ca}(kJ/mol) (kJ/mol)	ΔE_{Mg}(kJ/mol) (kJ/mol)
Cropland	0.1	8.999	7.486	8.707
	1	3.348	2.288	3.021
	10	0	0	0
21-Yr soil	0.1	8.555	7.172	8.102
	1	3.321	2.095	2.982
	10	0	0	0
53-Yr soil	0.1	7.829	7.014	7.686
	1	2.940	1.447	2.934
	10	0	0	0

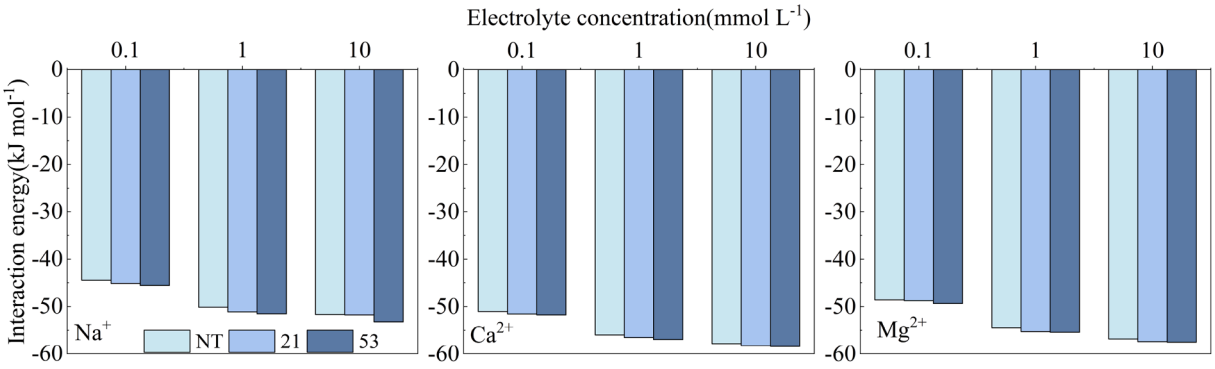

Fig. 6. Interaction energy between salt-based cations and the surface of soil particles in Cropland (NT), the 21-year-old *Robinia pseudoacacia* plantation area (21), and the 53-year-old *Robinia pseudoacacia* plantation area (53).

of fine soil particles, particularly fine sand, followed by clay (Hepper et al., 2006). As indicated in Table 1, the percentage of silt content in soil increases in succession with the length of vegetation restoration when compared with cropland: cropland soil (83.74 %) < 21-year-old *Robinia pseudoacacia* plantations soil (86.89 %) < 53-year-old *Robinia pseudoacacia* plantations soil (89.84 %). These results underscore the relationship between SSA and fine soil particles like fine silt. The negative contribution of clay to SCN might be mainly because the higher percentage of silt relative to clay in the tested soils (the number of silt particles being 3 to 6 times higher than clay) masked the clay's contribution to SCN. Tang et al. (2015) demonstrated through experimentation that soil clay content less than 1 μm in diameter is positively correlated with SCN, which differs from the current study's findings of a negative correlation between clay content (<20 μm) and SCN. The discrepancy may be due to the dominant clay minerals in their tested soils being montmorillonite and vermiculite, while ours consisted mostly of illite. The inherent charge variation among these minerals inevitably influences the contribution of soil particle size composition to the quantity of particle surface charge. The above analysis indicates that prolonged vegetation recovery increases SOM and soil clay content, enhancing SSA and SCN levels. Consequently, vegetation restoration directly impacts soil's fundamental physicochemical properties, which in turn influence its surface characteristics.

4.3. Electrochemical analysis of the evolution of base-cation adsorption characteristics at the soil–water interface during artificial Robinia pseudoacacia restoration

Based on soil electric field theory, the adsorption of base cations to the soil surface is essentially an ionic diffusion process driven by both the electric potential gradient and the concentration gradient (Li et al., 2010; Li et al., 2021a). The study results indicate that the SCN increases as the forest age of *Robinia pseudoacacia* progresses (Table 3); and at the given electrolyte concentration, the adsorption rates and equilibrium adsorption amounts of various ions also increase with the age of the *Robinia pseudoacacia* forest (Fig. 4). Soil surface charge is the basis driving the ion diffusion at the solid–liquid interface; as denoted by Fig. 7 ($P < 0.05$), there exists a significant positive linear relationship between SCN and the interface adsorption rate and equilibrium adsorption amount of base cations. This illustrates that the greater the charge on the soil particle surface, the stronger the driving force in the adsorption process of base cations, resulting in greater equilibrium adsorption amounts and adsorption rates of ions. Additionally, with the aging of the *Robinia pseudoacacia* forest, there is an increase in SSA (Table 3), meaning an increase in soil surface area and surface active sites. In other words, the increase in SSA during the vegetation restoration process leads to more ion adsorption active sites on the soil surface, thereby increasing the equilibrium adsorption amount of ions. Therefore, compared to cropland soil, the equilibrium adsorption amounts and adsorption rates of the base cations Na^+, Ca^{2+}, and Mg^{2+} on the surface of soil particles under all treatments increase with the growing age of the *Robinia pseudoacacia* forest. Overall, the soil surface properties such as SSA and SCN, along with the adsorption kinetic parameters, including the equilibrium adsorption capacity and the adsorption rate, show a significant positive correlation. It can be inferred that during vegetation restoration, as the recovery time increases, both SSA and SCN of the soil increase, thus accelerating the time required for ion adsorption to reach equilibrium.

The change in soil surface charge properties is the material basis affecting the kinetics of ionic interface reactions, while the ion-surface interactions regulated by surface electronegativity serve as the direct driving force for ion adsorption. As shown in Fig. 6, under a given ion type and concentration, the interaction energy between all ions and soil particles increases with the increase in years of vegetation restoration. For example, when the electrolyte concentration is 10 mmol/L, the adsorption energy of Na^+, Ca^{2+}, and Mg^{2+} on the soil surface planted with 21-year-old *Robinia pseudoacacia* increases by 0.213 %, 0.726 %, and 0.985 %, respectively, compared to cropland soil, while on the soil surface planted with 53-year-old *Robinia pseudoacacia*, the adsorption energy increases by 3.037 %, 1.003 %, and 1.143 %, respectively. Additionally, the adsorption energies of Na^+, Ca^{2+}, and Mg^{2+} on the soil surface increased the most on the soil surface planted with 53-year-old *Robinia pseudoacacia*, which increased by 3.037 % (10 mmol/L), 1.805 % (1 mmol/L), and 1.670 % (1 mmol/L), respectively. This means that the response of ion-soil particle interactions to variations in ion concentration varies depending on the land use pattern. The overall trend, however, is that when the concentration of base cations increases, their shielding effect on the surface negative charge will enhance, leading to a gradual decrease in the impact of soil particle surface charge on the diffusion process of cations from the liquid phase to the solid surface. As such, when electrolyte concentration is increased from 0.1 mmol/L to 10 mmol/L, the contribution rate of SCN to the kinetic parameters of base cation interface adsorption drops from 93.6 % to 3.8 %, while the contribution of SSA becomes more prominent, increasing from 2.6 % to 95.4 % (Table 5).

Under identical electrolyte concentration conditions (excluding 10 mmol/L), the diffusion activation energies for the three ions generally follow the order of cropland soil > 21-year-old *Robinia pseudoacacia* plantations soil > 53-year-old *Robinia pseudoacacia* plantations soil, with a significant negative linear correlation observed between SCN and ΔE_i ($P < 0.05$; Fig. 8). This correlation indicates that the stronger the electronegativity of the soil particle surface, the lower the diffusion activation energy required by base cations to adsorb onto the surface. Under the same electrolyte concentrations, the activation energies required for adsorption of Na^+, Ca^{2+}, and Mg^{2+} base cations on the loess soil surface exhibited marked differences with the age of the *Robinia pseudoacacia* forest (Table 6). The difference in diffusion activation energy between the monovalent ion Na^+ and the divalent ions Ca^{2+} and Mg^{2+} is primarily due to their differing ionic valences. In contrast, differences between divalent ions may be principally attributed to new forces

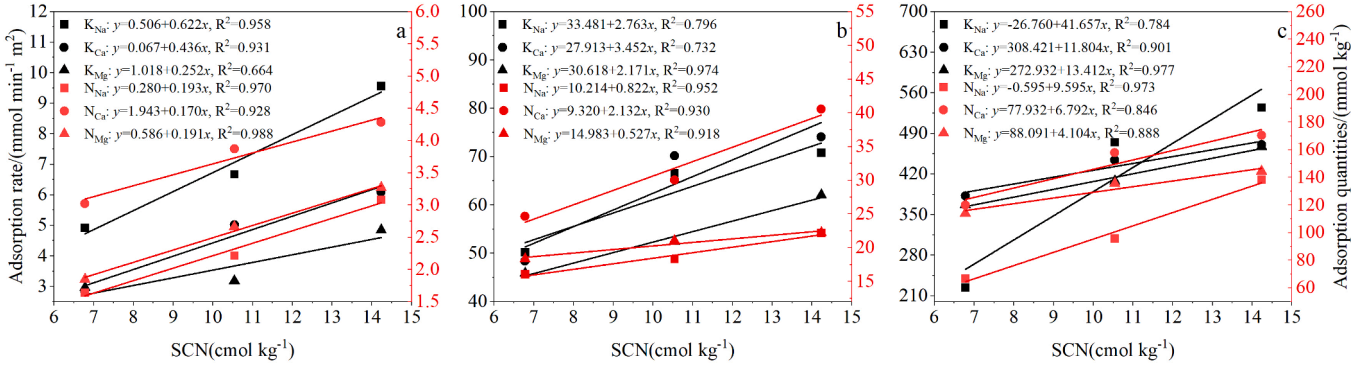

Fig. 7. Relationship between SCN and the adsorption rate and equilibrium adsorption of each ion (a: 0.1 mmol/L; b: 1 mmol/L; c: 10 mmol/L).

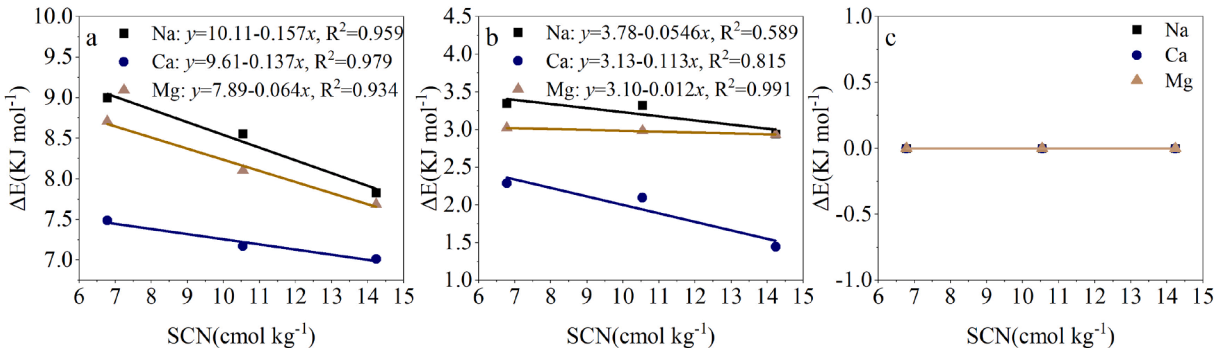

Fig. 8. Activation energies of Na^+, Ca^{2+}, and Mg^{2+} at the soil surface versus SCN (a: 0.1 mmol/L; b: 1 mmol/L; c: 10 mmol/L).

produced under the influence of the electric field. This is a significant driving force for the differentiated adsorption of ions with the same valence on charged soil surfaces (Du et al., 2020; Li et al., 2021b). Within soils of the same forest age, ΔE_i for the given base cation decreases with the increased concentration of the exchange solution (Table 6). When ions have high concentrations (activity), their chemical potential is also elevated; hence, the activation energy required for exchange adsorption is lowered, accelerating the cationic diffusion rate. As the ion concentration rises to 10 mmol/L, the energy barrier that needs to be overcome for the ion diffusion process in the system is reduced to zero, at which point ion exchange adsorption achieves complete equilibrium.

Under the conditions of the given electrolyte type and concentration, the interaction energy between ions and soil particles rises with the increase in vegetation recovery time, but the activation energy required for ion diffusion decreases with the increase in vegetation recovery time, resulting in a climb in the adsorption rate and equilibrium adsorption capacity of ions on the surface of soil particles. In the process of vegetation restoration, the improvement of ion adsorption and exchange performance of soil colloids can realize the adsorption and retention of nutrient ions in soil, reduce the loss of nutrients caused by rainfall, irrigation, or surface runoff, and finally achieve the purpose of improving soil fertilizer retention and fertilizer supply characteristics.

5. Conclusions

The restoration process of artificial *Robinia pseudoacacia* forests can lead to increases in soil organic matter and silt content while decreasing the pH and carbonate content; specific surface area and soil charge number increases; and soil electric field strength decreases. Clay particles (explanation rate of 51.2 %), silt particles (explanation rate of 13.7 %), and organic matter (explanation rate of 6.7 %) are the dominant controlling factors in the evolution of soil surface electrochemical properties during *Robinia pseudoacacia* forest recovery. Meanwhile, specific surface area and soil charge number are the main controlling factors influencing the adsorption kinetic differences of base cations Na^+, Ca^{2+}, and Mg^{2+} at the soil–water interface. Under given ionic types and concentration conditions, the adsorption rate and equilibrium adsorption amount of base cations increase with the growing age of *Robinia pseudoacacia* forests. This represents an increase in the quantity of soil surface charge and the ion-surface interaction energy during the vegetative restoration process, which in turn causes the diffusion activation energy barrier of ions to decrease successively over the recovery period, indicating that cationic diffusion activation energy follows cropland soil > 21-year-old *Robinia pseudoacacia* plantations soil > 53-year-old *Robinia pseudoacacia* plantations soil. Given a particular electrolyte concentration, the sequence of diffusion activation energies for different base cations on the same forest-age soil surface is $Na^+ > Mg^{2+} > Ca^{2+}$. Therefore, the order of equilibrium adsorption amounts follows: $Ca^{2+} > Mg^{2+} > Na^+$. Differences in ionic valence and new interactive forces between ions and soil particles induced by electric fields may be the reasons triggering the aforementioned results.

This study presents a novel concept for the utilization of artificial *Robinia pseudoacacia* forests in the ecological restoration of the Loess Plateau. It establishes a connection between *meso*-scale ion adsorption and the macroscopic process of ecological restoration through an electrochemical driving mechanism. The research findings can serve as a theoretical foundation for nutrient management in artificial forests, land fertility utilization, and the scientific evaluation of ecological restoration projects on the Loess Plateau.

CRediT authorship contribution statement

Zhiying Zhou: Writing – review & editing, Writing – original draft, Software, Investigation, Data curation. **Yajun Yang:** Writing – review & editing, Writing – original draft, Software, Investigation, Data curation. **Yizhe Yang:** Resources, Data curation. **Bokun Chang:** Software, Methodology, Investigation. **Xiaodong Yang:** Software, Methodology, Investigation. **Gang Cao:** Software, Methodology, Investigation. **Feinan Hu:** Validation, Supervision. **Chenyang Xu:** Validation, Supervision. **Xiaoli Liang:** Resources, Investigation. **Ling Qiu:** Resources. **Jialong Lv:** Resources, Project administration, Funding acquisition. **Wei Du:** Writing – review & editing, Supervision, Resources, Project administration, Funding acquisition, Conceptualization.

Declaration of competing interest

The authors declare that they have no known competing financial interests or personal relationships that could have appeared to influence the work reported in this paper.

Data availability

Data will be made available on request.

Acknowledgements

This work was supported by the Natural Science Basic Research Program of Shaanxi Province, China (No. 2021JQ-170), the National Natural Science Foundation of China (Nos. 42077135 and 42107332), the Agricultural Science and Technology Innovation Plan of Shaanxi Province, China (NYKJ-2022-YL(XN)39), and the Agricultural Key-scientific and Core-technological Project of Shaanxi Province, China (2023NYGG011).

References

Akpa, S.I., Odeh, I.O., Bishop, T.F., Hartemink, A.E., 2014. Digital mapping of soil particle-size fractions for Nigeria. Soil Sci. Soc. Am. J. 78, 1953–1966.

An, S.-S., Huang, Y.-M., Zheng, F.-L., 2009. Evaluation of soil microbial indices along a revegetation chronosequence in grassland soils on the Loess Plateau, Northwest China. Appl. Soil Ecol. 41, 286–292.
An, S., Mentler, A., Mayer, H., Blum, W.E., 2010. Soil aggregation, aggregate stability, organic carbon and nitrogen in different soil aggregate fractions under forest and shrub vegetation on the Loess Plateau, China. Catena 81, 226–233.
Asadu, C., Diels, J., Vanlauwe, B., 1997. A comparison of the contributions of clay, silt, and organic matter to the effective cec of soils of subsaharan africa. Soil Sci. 162, 785–794.
Bardgett, R.D., Wardle, D.A., 2003. Herbivore-mediated linkages between aboveground and belowground communities. Ecology 84, 2258–2268.
Bolan, N.S., Naidu, R., Syers, J.K., Tillman, R.W., 1999. Surface charge and solute interactions in soils. Adv. Agron. 67, 87–140.
Bronick, C.J., Lal, R., 2005. Soil structure and management: a review. Geoderma 124, 3–22.
Cao, C., et al., 2008. Soil chemical and microbiological properties along a chronosequence of Caragana microphylla Lam. plantations in the Horqin sandy land of Northeast China. Appl. Soil Ecol. 40, 78–85.
Chen, S., et al., 2018. Plant diversity enhances productivity and soil carbon storage. Proc. Natl. Acad. Sci. 115, 4027–4032.
Deng, L., et al., 2019. Drivers of soil microbial metabolic limitation changes along a vegetation restoration gradient on the Loess Plateau, China. Geoderma 353, 188–200.
Deng, L., Liu, G.b., Shangguan, Z.p., 2014. Land-use conversion and changing soil carbon stocks in China's 'Grain-for-Green'Program: a synthesis. Global change biology, 20, 3544-3556.
Deng, H., Li, H., 2022. Specific cation effects on surface reactions of HgCl2 in clay-water systems. Appl. Clay Sci. 224, 106523.
Dijkstra, F.A., Carrillo, Y., Pendall, E., Morgan, J.A., 2013. Rhizosphere priming: a nutrient perspective. Front. Microbiol. 4, 216.
Du, W., et al., 2017. Estimating Hofmeister energy in ion-clay mineral interactions from the Gouy-Chapman theory. Appl. Clay Sci. 146, 122–130.
Du, W., et al., 2019. Theory to describe incomplete ion exchange in charged heterogeneous systems. J. Soil. Sediment. 19, 1839–1849.
Du, W., et al., 2020. Specific ion effects of incomplete ion-exchange by electric field-induced ion polarization. RSC Adv. 10, 15190–15198.
Du, W., et al., 2021. Combined determination analysis of surface properties evolution towards bentonite by pH treatments. Colloids Surf A Physicochem Eng Asp 626, 127067.
Du, W., Li, R., Liu, X.-M., Tian, R., Li, H., 2016. Specific ion effects on ion exchange kinetics in charged clay. Colloids Surf A Physicochem Eng Asp 509, 427–432.
Ersahin, S., Gunal, H., Kutlu, T., Yetgin, B., Coban, S., 2006. Estimating specific surface area and cation exchange capacity in soils using fractal dimension of particle-size distribution. Geoderma 136, 588–597.
Fu, S., Zou, X., Coleman, D., 2009. Highlights and perspectives of soil biology and ecology research in China. Soil Biol. Biochem. 41, 868–876.
Ghani, M.I., et al., 2023. Variations of soil organic carbon fractions in response to conservative vegetation successions on the Loess Plateau of China. Int. Soil Water Conserv. Res. 11, 561–571.
Gruba, P., Mulder, J., 2015. Tree species affect cation exchange capacity (CEC) and cation binding properties of organic matter in acid forest soils. Sci. Total Environ. 511, 655–662.
Gu, C., et al., 2019. Influence of vegetation restoration on soil physical properties in the Loess Plateau, China. J. Soil. Sediment. 19, 716–728.
Han, M., Sun, L., Gan, D., Fu, L., Zhu, B., 2020. Root functional traits are key determinants of the rhizosphere effect on soil organic matter decomposition across 14 temperate hardwood species. Soil Biol. Biochem. 151, 108019.
Hepper, E.N., Buschiazzo, D.E., Hevia, G., Urioste, A., Antón, L., 2006. Clay mineralogy, cation exchange capacity and specific surface area of loess soils with different volcanic ash contents. Geoderma 135, 216–223.
Huang, C., Zeng, Y., Wang, L., Wang, S., 2020. Responses of soil nutrients to vegetation restoration in China. Reg. Environ. Chang. 20, 1–12.
Iturri, L.A., Buschiazzo, D.E., 2014. Cation exchange capacity and mineralogy of loess soils with different amounts of volcanic ashes. Catena 121, 81–87.
Jardine, P.M., Sparks, D.L., 1984. Potassium-Calcium Exchange in a Multireactive Soil System: I. Kinetics. Soil Sci. Soc. Am. J. 48, 39–45.
Jiao, F., Wen, Z.-M., An, S.-S., 2011. Changes in soil properties across a chronosequence of vegetation restoration on the Loess Plateau of China. Catena 86, 110–116.
Jin, Z., et al., 2019. Valley reshaping and damming induce water table rise and soil salinization on the Chinese Loess Plateau. Geoderma 339, 115–125.
Jin, Z., et al., 2022. Soil pH changes in a small catchment on the Chinese Loess Plateau after long-term vegetation rehabilitation. Ecol. Eng. 175, 106503.
Johansson, M.-B., 1995. The chemical composition of needle and leaf litter from Scots pine, Norway spruce and white birch in Scandinavian forests. Forestry: an Int. J. Forest Res. 68, 49–62.
Kweon, G., Lund, E., Maxton, C., 2013. Soil organic matter and cation-exchange capacity sensing with on-the-go electrical conductivity and optical sensors. Geoderma 199, 80–89.
Lal, R., 2002. Soil carbon sequestration in China through agricultural intensification, and restoration of degraded and desertified ecosystems. Land Degrad. Dev. 13, 469–478.
Lei, D., Shangguan, Z.-P., Rui, L., 2012. Effects of the grain-for-green program on soil erosion in China. Int. J. Sedim. Res. 27, 120–127.
Li, H., et al., 2011a. Combined determination of specific surface area and surface charge properties of charged particles from a single experiment. Soil Sci. Soc. Am. J. 75, 2128–2135.
Li, R., et al., 2011b. Analytical models for describing cation adsorption/desorption kinetics as considering the electrostatic field from surface charges of particles. Colloids Surf A Physicochem Eng Asp 392, 55–66.
Li, B., et al., 2023a. Effects of vegetation restoration on soil nitrogen fractions and enzyme activities in arable land on purple soil slopes. Plants 12, 4188.
Li, S., et al., 2023c. Soil particle aggregation and aggregate stability associated with ion specificity and organic matter content. Geoderma 429, 116285.
Li, H., Li, R., Zhu, H., Wu, L., 2010. Influence of electrostatic field from soil particle surfaces on ion adsorption–diffusion. Soil Sci. Soc. Am. J. 74, 1129–1138.
Li, R., Li, H., Zhu, H., Wu, L., 2011c. Kinetics of cation adsorption on charged soil mineral as strong electrostatic force presence or absence. J. Soil. Sediment. 11, 53–61.
Li, Q., Li, R., Shi, W., 2021a. Cation adsorption at permanently (montmorillonite) and variably (quartz) charged mineral surfaces: Mechanisms and forces from subatomic scale. Appl. Clay Sci. 213, 106245.
Li, D., Niu, S., Luo, Y., 2012. Global patterns of the dynamics of soil carbon and nitrogen stocks following afforestation: a meta-analysis. New Phytol. 195, 172–181.
Li, Y.Y., Shao, M.A., 2006. Change of soil physical properties under long-term natural vegetation restoration in the Loess Plateau of China. J. Arid Environ. 64, 77–96.
Li, Q., Shi, W., Yang, Q., 2021b. Polarization induced covalent bonding: A new force of heavy metal adsorption on charged particle surface. J. Hazard. Mater. 412, 125168.
Li, Q., Tian, R., Yang, Q., 2023b. Insight into mechanisms of heavy metal-induced natural clay aggregation. Appl. Clay Sci. 231, 106746.
Li, X., Yin, X., Wang, Z., Fan, W., 2015. Litter mass loss and nutrient release influenced by soil fauna of Betula ermanii forest floor of the Changbai Mountains, China. Appl. Soil Ecol. 95, 15–22.
Li, Y., Zhu, Y., Ding, W., Liu, X., Li, H., 2022. An analytical approach to estimating electrostatic repulsion between soil particles. Soil Tillage Res. 223, 105488.
Ließ, M., Glaser, B., Huwe, B., 2012. Uncertainty in the spatial prediction of soil texture: comparison of regression tree and Random Forest models. Geoderma 170, 70–79.
Liu, J., et al., 2020a. Soil organic matter and silt contents determine soil particle surface electrochemical properties across a long-term natural restoration grassland. Catena 190, 104526.
Liu, D., Du, W., Liu, X., Tian, R., Li, H., 2019. To distinguish Electrostatic, coordination bond, nonclassical polarization, and dispersion forces on cation–clay interactions. J. Phys. Chem. C 123, 2157–2164.
Liu, D., Tian, R., Liu, X., Li, H., 2023. Polarization induced covalent/hydrogen bonding adsorption of NH4+ and K+ in soils: comparison study on permanently and variably charged soils. J. Soil. Sediment. 1–10.
Liu, X., Yang, T., Li, H., Wu, L., 2020b. Effects of interactions between soil particles and electrolytes on saturated hydraulic conductivity. Eur. J. Soil Sci. 71, 190–203.
Liu, J., Yang, Y., Zheng, Q., Su, X., Zhou, Z., 2022. Response of soil aggregate stability and rill erodibility to soil electric field. Catena 215, 106338.
Long, Z., et al., 2024. Bio-accessibility and mobilization dynamics of soil vanadium during a 48-year vegetation restoration in a vanadium titano-magnetite tailings reservoir. Sci. Total Environ. 906, 167507.
Lv, P., et al., 2021. Soil net nitrogen transformation rates are co-determined by multiple factors during the landscape evolution in Horqin Sandy land. Catena 206, 105576.
Lv, P., et al., 2023. Effects of altered precipitation patterns on soil nitrogen transformation in different landscape types during the growing season in northern China. Catena 222, 106813.
Ma, Y., et al., 2023. Global patterns of rhizosphere effects on soil carbon and nitrogen biogeochemical processes. Catena 220, 106661.
Ma, R., Hu, F., Xu, C., Liu, J., Zhao, S., 2022. Response of soil aggregate stability and splash erosion to different breakdown mechanisms along natural vegetation restoration. Catena 208, 105775.
Murty, D., Kirschbaum, M.U., Mcmurtrie, R.E., Mcgilvray, H., 2002. Does conversion of forest to agricultural land change soil carbon and nitrogen? A review of the literature. Glob. Chang. Biol. 8, 105–123.
Nelson, D.a., Sommers, L.E., 1983. Total carbon, organic carbon, and organic matter. Methods of soil analysis: Part 2 chemical and microbiological properties, 9, 539-579.
Oorts, K., Vanlauwe, B., Merckx, R., 2003. Cation exchange capacities of soil organic matter fractions in a Ferric Lixisol with different organic matter inputs. Agr Ecosyst Environ 100, 161–171.
Pennell, K., Abriola, L., Boyd, S., 1995. Surface area of soil organic matter reexamined. Soil Sci. Soc. Am. J. 59, 1012–1018.
Saidian, M., Godinez, L.J., Prasad, M., 2016. Effect of clay and organic matter on nitrogen adsorption specific surface area and cation exchange capacity in shales (mudrocks). J. Nat. Gas Sci. Eng. 33, 1095–1106.
Shang, S., et al., 2014. Soil organic carbon in particle size and density fractionations under four forest vegetation-land use types in subtropical China. Forests 5, 1391–1408.
Soares, M.R., Alleoni, L.R., Vidal-Torrado, P., Cooper, M., 2005. Mineralogy and ion exchange properties of the particle size fractions of some Brazilian soils in tropical humid areas. Geoderma 125, 355–367.
Sparrius, L., Sevink, J., Kooijman, A., 2012. Effects of nitrogen deposition on soil and vegetation in primary succession stages in inland drift sands. Plant and Soil 353, 261–272.
Su, H., Kang, W., Li, Y., Li, Z., 2021. Fluoride and nitrate contamination of groundwater in the Loess Plateau, China: sources and related human health risks. Environ. Pollut. 286, 117287.
Sumner, M.E., Miller, W.P., 1996. Cation exchange capacity and exchange coefficients. Methods of soil analysis. Part 3 Chemical Methods 5, 1201–1229.
Sun, C., Liu, G., Xue, S., 2016. Land-use conversion changes the multifractal features of particle-size distribution on the Loess Plateau of China. Int. J. Environ. Res. Public Health 13, 785.

Tang, Y., Li, H., Liu, X., Zhu, H., Tian, R., 2015. Unraveling the size distributions of surface properties for purple soil and yellow soil. J. Environ. Sci. 32, 81–89.
Tsao, T., et al., 2013. Separation and identification of soil nanoparticles by conventional and synchrotron X-ray diffraction. Appl. Clay Sci. 85, 1–7.
Tuo, D., et al., 2018. Effects of revegetation and precipitation gradient on soil carbon and nitrogen variations in deep profiles on the Loess Plateau of China. Sci. Total Environ. 626, 399–411.
Van Veen, J., Kuikman, P., 1990. Soil structural aspects of decomposition of organic matter by micro-organisms. Biogeochemistry 11, 213–233.
Vittori Antisari, L., Falsone, G., Carbone, S., Vianello, G., 2013. Short-term effects of forest recovery on soil carbon and nutrient availability in an experimental chestnut stand. Biol. Fertil. Soils 49, 165–173.
Wang, Q., et al., 2021. Absorptive and transport roots differ in terms of their impacts on rhizosphere soil carbon storage and stability in alpine forests. Soil Biol. Biochem. 161, 108379.
Wang, C., et al., 2023. Vegetation restoration of abandoned cropland improves soil phosphorus availability and microbial activities in the Danxia degraded region. Appl. Soil Ecol. 188, 104921.
Wang, Y., Shao, M.a., Zhu, Y., Liu, Z., 2011. Impacts of land use and plant characteristics on dried soil layers in different climatic regions on the Loess Plateau of China. Agric. Forest Meteorol., 151, 437-448.
Wang, D., Fu, B., Zhao, W., Hu, H., Wang, Y., 2008. Multifractal characteristics of soil particle size distribution under different land-use types on the Loess Plateau, China. Catena 72, 29–36.
Wang, H., Zhang, G.-H., Li, N.-N., Zhang, B.-J., Yang, H.-Y., 2018. Soil erodibility influenced by natural restoration time of abandoned farmland on the Loess Plateau of China. Geoderma 325, 18–27.
Wen, J., Wu, Y., Lan, M., Li, X., 2023. Influence mechanism of plant litter mediated reduction of iron and sulfur on migration of potentially toxic elements from mercury-thallium mine waste. Environ. Pollut. 121742.
Yang, X., et al., 2015. Determination of soil texture by laser diffraction method. Soil Sci. Soc. Am. J. 79, 1556–1566.
Yang, B., Wang, R., Xiao, H., Cao, Q., Liu, T., 2018. Spatio-temporal variations of soil water content and salinity around individual Tamarix ramosissima in a semi-arid saline region of the upper Yellow River, Northwest China. J. Arid. Land 10, 101–114.
Yu, Z.H., Zhang, J.B., Zhang, C.Z., Xin, X.L., Li, H., 2017. The coupling effects of soil organic matter and particle interaction forces on soil aggregate stability. Soil Tillage Res. 174, 251–260.
Zeng, Q., Darboux, F., Man, C., Zhu, Z., An, S., 2018. Soil aggregate stability under different rain conditions for three vegetation types on the Loess Plateau (China). Catena 167, 276–283.
Zhai, J., et al., 2020. Change in soil particle size distribution and erodibility with latitude and vegetation restoration chronosequence on the Loess Plateau, China. Int. J. Environ. Res. Public Health 17, 822.
Zhang, C., Xue, S., Liu, G.-B., Song, Z.-L., 2011. A comparison of soil qualities of different revegetation types in the Loess Plateau, China. Plant and Soil 347, 163–178.
Zhang, C., Liu, G., Xue, S., Wang, G., 2016. Soil bacterial community dynamics reflect changes in plant community and soil properties during the secondary succession of abandoned farmland in the Loess Plateau. Soil Biol. Biochem. 97, 40–49.
Zhao, Z., et al., 2019. Evolution of soil surface charge in a chronosequence of paddy soil derived from Alfisol. Soil Tillage Res. 192, 144–150.
Zhao, Y.-G., Liu, X.-F., Wang, Z.-L., Zhao, S.-W., 2015. Soil organic carbon fractions and sequestration across a 150-yr secondary forest chronosequence on the Loess Plateau, China. Catena 133, 303–308.
Zhong, Y., Yan, W., Wang, R., Shangguan, Z., 2017. Differential responses of litter decomposition to nutrient addition and soil water availability with long-term vegetation recovery. Biol. Fertil. Soils 53, 939–949.
Zhou, W., Li, C., Wang, S., Ren, Z., Stringer, L.C., 2023. Effects of vegetation restoration on soil properties and vegetation attributes in the arid and semi-arid regions of China. J. Environ. Manage. 343, 118186.
Zhu, Y., Wang, Y., Chen, L., 2019. Responses of ground-active arthropods to black locust (Robinia pseudoacacia L.) afforestation in the Loess Plateau of China. Catena 183, 104233.
Zuo, X., et al., 2009. Spatial heterogeneity of soil properties and vegetation–soil relationships following vegetation restoration of mobile dunes in Horqin Sandy Land, Northern China. Plant and Soil 318, 153–167.